Large-scale exploratory analysis of the spatiotemporal distribution of climate projections: applying the STRIVIng toolbox

Diaz, Vitali; Corzo, Gerald A.; Pérez, José R.

DOI
10.1016/B978-0-12-811689-0.00003-3

Publication date
2019

Document Version
Final published version

Published in
Spatiotemporal Analysis of Extreme Hydrological Events

3

Large-Scale Exploratory Analysis of the Spatiotemporal Distribution of Climate Projections: Applying the STRIVIng Toolbox

Vitali Diaz[1,2], Gerald Corzo[1], José R. Pérez[3]

[1]UNESCO-IHE INSTITUTE FOR WATER EDUCATION, DELFT, THE NETHERLANDS; [2]WATER RESOURCES SECTION, DELFT UNIVERSITY OF TECHNOLOGY, DELFT, THE NETHERLANDS; [3]INSTITUTO NACIONAL DE RECURSOS HIDRÁULICOS (INDRHI), SANTO DOMINGO, DOMINICAN REPUBLIC

1. Introduction

Precipitation and temperature projections over the next few decades indicate that on earth their spatiotemporal distribution will undergo changes (IPCC, 2014; Moss et al., 2010; Najafi and Moradkhani, 2015; Taylor et al., 2012). These variations might modify the way in which extreme hydrological events (EHEs) occur, affecting their frequency and intensity (e.g., Coumou and Rahmstorf, 2012; Trenberth, 2012). Because EHEs, such as droughts and floods, have a great negative impact on human activities, a better understanding of the expected spatiotemporal variability of precipitation and temperature is necessary.

Relatively recent studies have been carried out to analyze the spatiotemporal changes of future precipitation and temperature considering the entire planet or a number of continents (e.g., Boer, 2009; Hawkins and Sutton, 2009; Milly et al., 2005). There are also applications at lower scales (e.g., Wang et al., 2016). These data have been considered a challenge for big data in many studies. This relates to the amount of information that can be handled and the processes involved in the analysis.

In this study we present an analysis using the Spatio-TempoRal distribution and Interannual VarIability of projections (STRIVIng) toolbox for statistical exploratory analysis of future precipitation and temperature. The toolbox provides a set of elements for numerical and visual comparison of the baseline and projections. STRIVIng is designed to work with monthly values and various spatial resolutions. In this document, large-scale applications are presented following a standard step-by-step exploratory analysis.

Spatiotemporal Analysis of Extreme Hydrological Events. https://doi.org/10.1016/B978-0-12-811689-0.00003-3

To illustrate the use of STRIVIng, three case studies were undertaken: Dominican Republic, Mexico, and Amazon basin, to try to cover regions of different sizes. Following this introductory section, concepts and the description of the toolbox are shown. Subsequently, data, case studies, and the application are described. Finally, results and conclusions are presented.

2. Framework (Global Climate Model Projections)

A type of model to simulate climate is the so-called General Circulation Model (GCMs), which makes use of mathematical formulations to reproduce the general circulation of the atmosphere. To analyze the possible implications of the human and natural influences over climate, GCMs are forced, in a systematic way, to analyze possible futures under the scenarios approach (Moss et al., 2010). In this way, climate projections are estimated for each scenario. The design of scenarios and GCM setups are coordinated worldwide by the Coupled Model Intercomparison Project (CMIP), where several modeling teams participate (Meehl et al., 2014).

Projection data are available for each GCM and each scenario. Due to the information of these variables is usually on a coarse spatial and temporal scale, in addition to presenting a deviation in value compared to ground observations, at least two steps are necessary before use: downscaling and bias correction. Downscaling refers to the procedure of changing the coarse scale to a finer one. Bias correction is the procedure of tuning simulated variables in the atmosphere with those gathered on the ground.

There are a couple of examples of research projects where the adjustment (i.e., downscaling and calibration) of P and T projections was within the scope: ENSEMBLES (ensembles-eu.metoffice.com) and Regional Climate, Water, Energy Resources and uncertainties (RIWER 2030 project; www.lthe.fr/RIWER 2030), where the target was Europe. Global research projects included the Integrated Project Water and Global Change (WATCH, www.eu-watch.org) and WorldClim (worldclim.org). From all these projects, data of adjusted P and T are freely available for download or on request.

As Meehl et al. (2014) point out "to better understand the past, present, and future climate, the state-of-the-art climate model simulations are compared to gain insights into the processes, mechanisms, and consequences of climate variability." One way to carry out this comparative analysis is through the examination of the statistics of adjusted climate variables, as well as the investigation of their expected spatial distribution. The toolbox introduced in this document helps to carry out comparative analysis. A description of the toolbox is given next.

3. STRIVIng Methodology

In general, the methodology involves two steps: processing and visualization (Fig. 3.1). In the first part, input data are processed to calculate the statistics and average values of

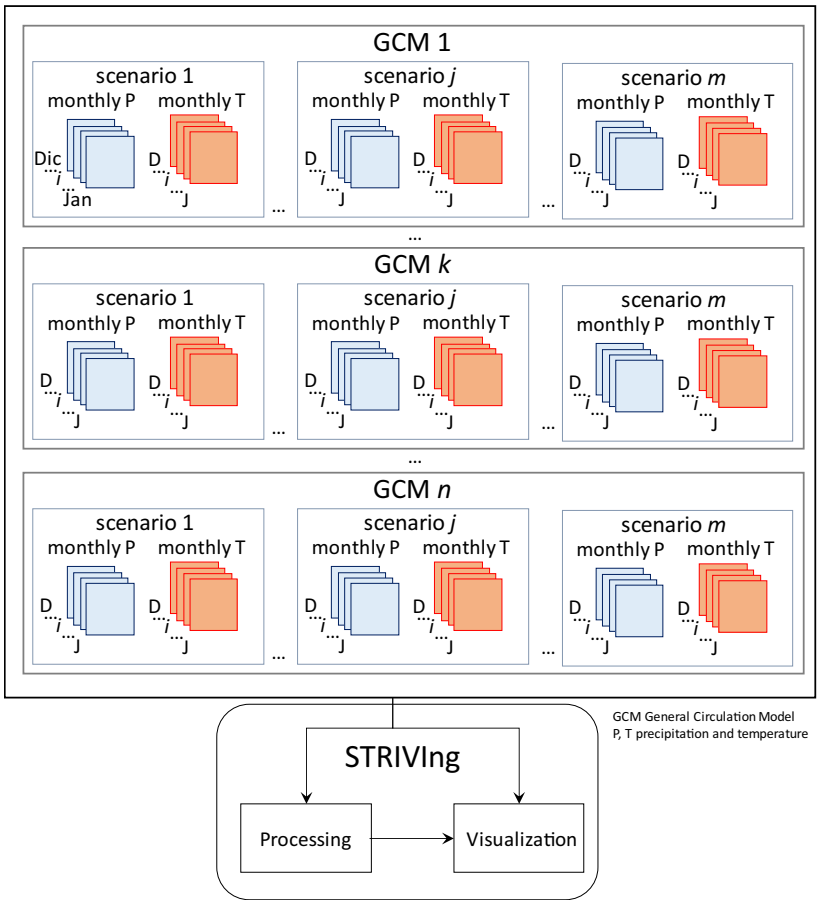

FIGURE 3.1 Schematic overview of the STRIVIng toolbox. *GCM*, General Circulation Model; *P*, precipitation; *T*, temperature.

adjusted projections for a study area. The second part consists of a set of graphic elements for the visualization of spatial distribution, as well as monthly average values of precipitation and temperature for the study area.

Regarding processing, consider that there are n GCMs (Fig. 3.1). Each kth GCM has the information of m scenarios. Each scenario, in turn, has data of the long-term mean precipitation and mean temperature by month from January to December (J to D). Also for each scenario, annual precipitation and temperature are available for reference and future periods. The long-term mean precipitation (Pm) and mean temperature (Tm) for the ith month and the jth scenario, also called ensemble mean, are calculated with Eqs. (3.1) and (3.2), respectively:

$$Pm_{i,j} = \frac{1}{n}\sum_{k=1}^{n} P_{i,j,k} \tag{3.1}$$

$$Tm_{i,j} = \frac{1}{n}\sum_{k=1}^{n} T_{i,j,k}. \tag{3.2}$$

The average annual P and T of the n GCMs for the jth scenario is computed with Eqs. (3.3) and (3.4), respectively:

$$Pan_j = \frac{1}{n}\sum_{k=1}^{n} Pa_{j,k} \tag{3.3}$$

$$Tan_j = \frac{1}{n}\sum_{k=1}^{n} Ta_{j,k}. \tag{3.4}$$

For the jth scenario, the average volume of annual P for a region is calculated with Eq. (3.5):

$$V_j = A \times Pan_j \tag{3.5}$$

where A is the region area.

The average values calculated with Eqs. (3.1)−(3.4), as well as the input, are examined through three graphic elements: image, line, and box-plot. The use of these graphs is shown in Section 5. In STRIVIng methodology, the inputs are the climate projections, and the elements to process and analyze these data are incorporated in the STRIVIng toolbox.

4. Data, Case Studies, and Experiment Setup

4.1 Data

To illustrate the use of STRIVIng, WorldClim data are used (Fick and Hijmans, 2017). These data were considered because they are available for direct download and their spatial resolution is lower than half a degree. A detailed description of data and the adjustment procedure can be found in Fick and Hijmans (2017) and at www.worldclim.org/downscaling.

WorldClim projections correspond to the fifth assessment of CMIP (IPCC, 2014). In CMIP5, four Representative Concentration Pathways (RCPs) of greenhouse gas (GHG) concentration trajectories are taken into account for climate modeling. RCPs refer to four likely climate futures where diverse amounts of GHG are emitted at different times. As Meinshausen et al. (2011) highlight "RCP 2.6 assumes that global annual GHG emissions peak between 2010-20, with emissions declining substantially thereafter. Emissions in RCP 4.5 peak around 2040, then decline. In RCP 6, emissions peak around 2080, then decline. In RCP 8.5, emissions continue to rise throughout the 21st century."

Table 3.1 WorldClim Data (Fick and Hijmans, 2017)

GCM	RCP 2.6	RCP 4.5	RCP 6.0	RCP 8.5
+ACCESS1-0		*		*
BCC-CSM1-1	*	*	*	*
CCSM4	*	*	*	*
CESM1-CAM5-1-FV2		*		
+CNRM-CM5	*	*		*
GFDL-ESM2G	*	*	*	
GFDL-CM3	*	*		*
GISS-E2-R	*	*	*	*
HadGEM2-AO	*	*	*	*
HadGEM2-ES	*	*	*	*
HadGEM2-CC		*		*
INMCM4		*		*
IPSL-CM5A-LR	*	*	*	*
+MIROC5	*	*	*	*
MRI-CGCM3	*	*	*	*
+MIROC-ESM-CHEM	*	*	*	*
MPI-ESM-LR	*	*		*
+MIROC-ESM	*	*	*	*
NorESM1-M	*	*	*	*

*, indicates the availability of data. +, for noncommercial use. GCM and RCP stand for General Circulation Model and Representative Concentration Pathway, respectively.

Future P and T of WorldClim (Table 3.1) are available for 19 GCMs, four RCPs (scenarios), and the aggregate periods of 2050 (2041–60) and 2070 (2061–80). Data are arranged in four spatial resolutions: 30 s ($\sim$1 km^2), 2.5 s ($\sim$20 km^2), 5 s ($\sim$80 km^2), and 10 min ($\sim$340 km^2 at the equator). The baseline information corresponds to the period 1950–2000. In this chapter, 10-min data of both baseline and projections were used for the large-scale applications presented hereafter.

4.2 Case Studies

For the application, two countries and one large basin were considered: Dominican Republic, Mexico, and Amazon basin (Fig. 3.2). The Amazon basin is located in the territories of Brazil, Bolivia, Peru, Ecuador, Colombia, Venezuela, Guyana, Suriname, and French Guiana. The Amazon River and its tributaries drain throughout this basin into the Atlantic Ocean. In Table 3.2, the main characteristics of the cases studies are presented.

4.3 Experiment Setup

P and T projections of the study areas were processed taking into account the 19 GCMs and four RCPs of WorldClim data, as well as the information of the baseline period of 1970–2000. In Section 6, some relevant findings are presented. To extract and process

FIGURE 3.2 Mexico, Dominican Republic, and Amazon basin location.

Table 3.2 Characteristics of Case study Areas

Case Study	Area (km^2)	Mean Annual Precipitation (mm)	Mean Annual Temperature (°C)
Dominican Republic[1]	48,315	1500	25
Mexico[2]	1,972,550	780	21
Amazon basin[3]	6,150,000	2500	24–26

Sources: (1) US Library of Congress; (2) National Meteorological Service (SMN, Abbreviation in Spanish), Mexico; (3) Food and Agriculture Organization of the United Nations (FAO).

the data, three masks were built with the same spatial resolution as the data, i.e., 10 min. Long-term mean P and T from January to December (J to D) were computed with Eqs. (3.1) and (3.2). The mean annual P and T were calculated by using Eqs. (3.3) and (3.4), respectively. To estimate the annual water volume with Eq. (3.5), the next areas where considered: Dominican Republic (48,670 km^2), Mexico (1,972,550 km^2), and Amazon

basin (6,171,148.7 km^2). These areas are slightly different from those reported in the sources (Table 3.2), but correspond to the shape files used for the construction of the masks. Water volumes are shown in billions of cubic meters (10^9 m^3).

5. Results and Discussion

5.1 Dominican Republic

For both periods 2050 (2041–60) and 2070 (2061–80), most GCMs agree that the greatest changes in the spatial distribution of *P* will occur on the north coast. While on the border with Haiti, the condition practically remains stable, Figs. 3.3 and 3.4, respectively. For the 2050 period, the northern coast will experience an increase in annual rainfall, while a decrease is expected on the southern coast. On the other hand, for the period of 2070, it is expected that on the north coast the magnitude of the annual rains will be of the same order as the historical ones. The south coast will experience a decrease with respect to those of the baseline period.

Fig. 3.5 shows that the long-term mean *P* for the 12 months, in general, will show a decrease in the coming decades, mainly in the months of May to October. June and July are the months that present the greatest fall. The May rainfall projection shows the greatest disagreement among GCMs.

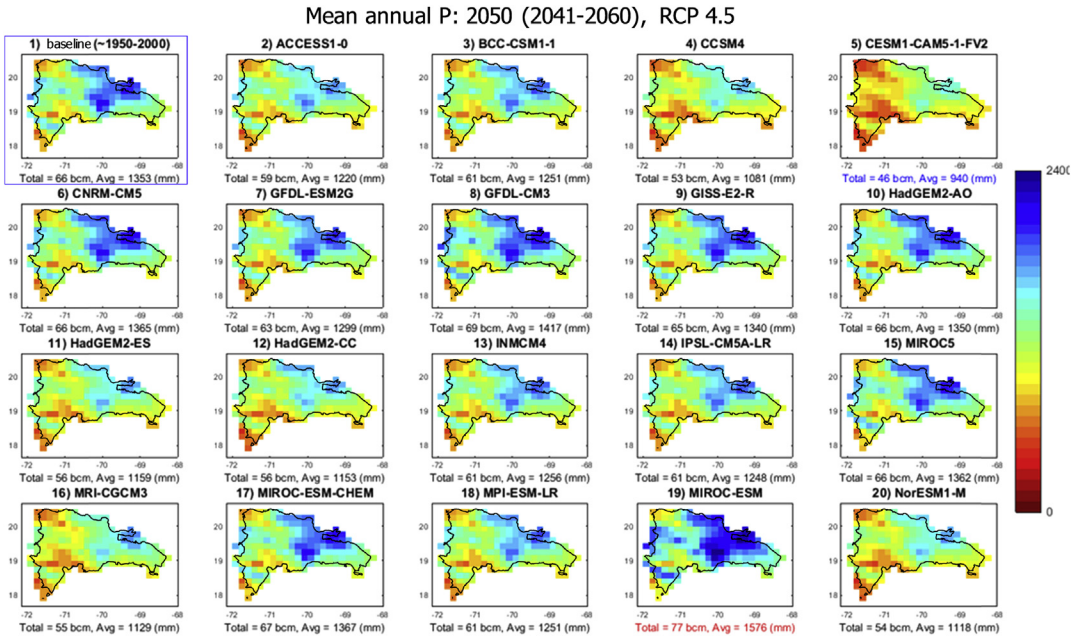

FIGURE 3.3 Spatial distribution of mean annual *P* (mm) over Dominican Republic for the period 2041–60 (2050): baseline and 19 GCMs, and RCP 4.5. *GCM*, General Circulation Model; *P*, precipitation; *RCP*, Representative Concentration Pathway.

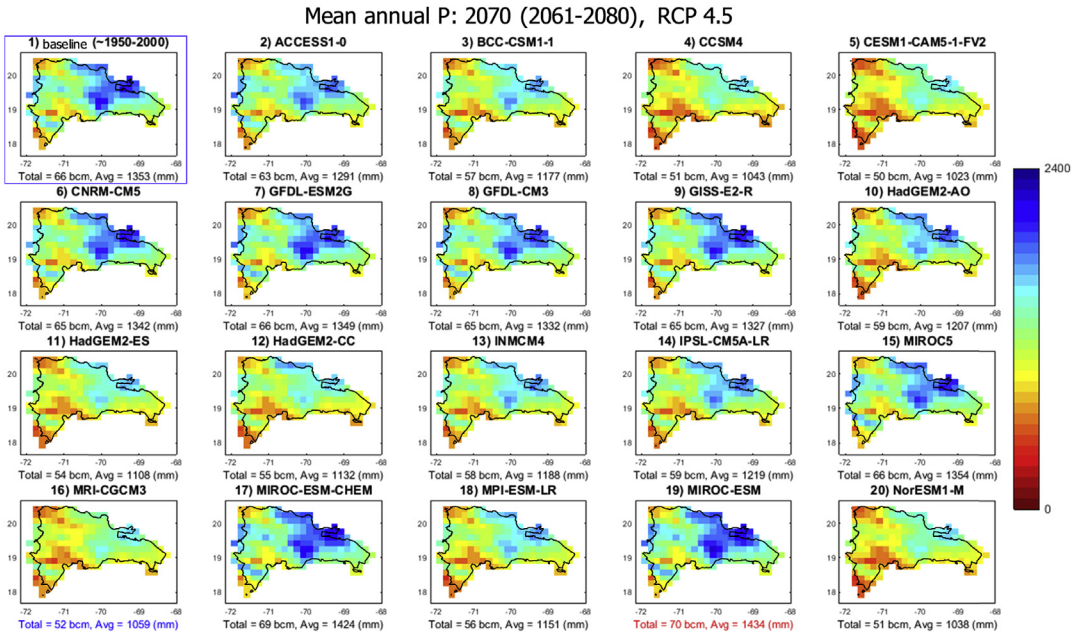

FIGURE 3.4 Spatial distribution of mean annual *P* (mm) over Dominican Republic for the period 2061–80 (2070): baseline and 19 GCMs, and RCP 4.5. *GCM*, General Circulation Model; *P*, precipitation; *RCP*, Representative Concentration Pathway.

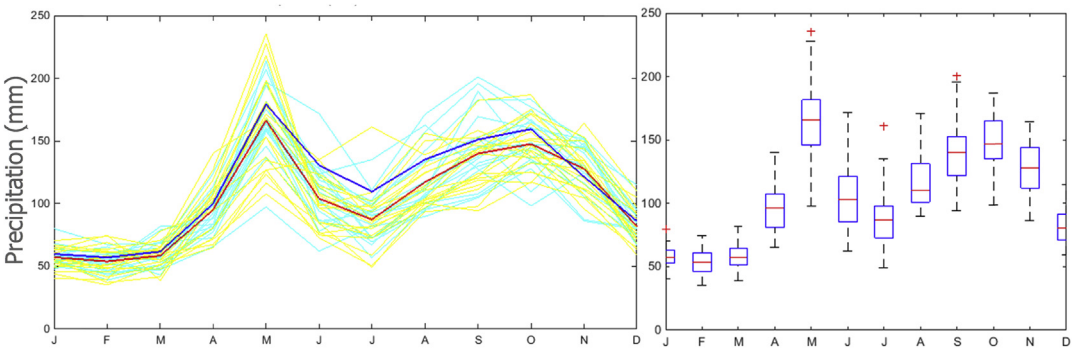

FIGURE 3.5 Dominican Republic. (*Left*) Long-term mean *P* of the baseline period (*solid blue line*) and 19 RCP 4.5 projections (*solid red line*). Long-term mean *P* of each projection is also displayed for the period 2041–60 (*solid cyan line*) and 2061–80 (*solid yellow line*). (*Right*) Box-plot with *P* projections of the two periods. *P*, Precipitation; *RCP*, Representative Concentration Pathway.

Regarding temperatures, Figs. 3.6 and 3.7 indicate that the country will suffer an increase in the mean annual values in practically the whole territory for the periods 2041–60 and 2061–80, respectively. Only in the central part will the condition remain more stable in both cases. Fig. 3.8 shows that the long-term mean *T* will increase to around 2 degrees in all 12 months.

5.2 Mexico

The spatial distribution of the mean annual *P* agrees with most of the GCMs for the period 2041–60 (Fig. 3.9). The maximum magnitudes of rainfall are observed on the south coast with the Gulf of Mexico and on the southwest coast with the Pacific Ocean. The lowest values are observed in the north and northwest of the country, on the border with the United States. The area with most disagreement is the southwest coast with the Pacific Ocean.

According to the four RCPs (Fig. 3.10), the long-term mean *P* of projections of the 12 months will remain with similar magnitude throughout the year, except for the months of June to September (J to S), where the models show mainly a drop in the values. July is the month that shows the greatest fall; this drop increases from RCP 2.6 to

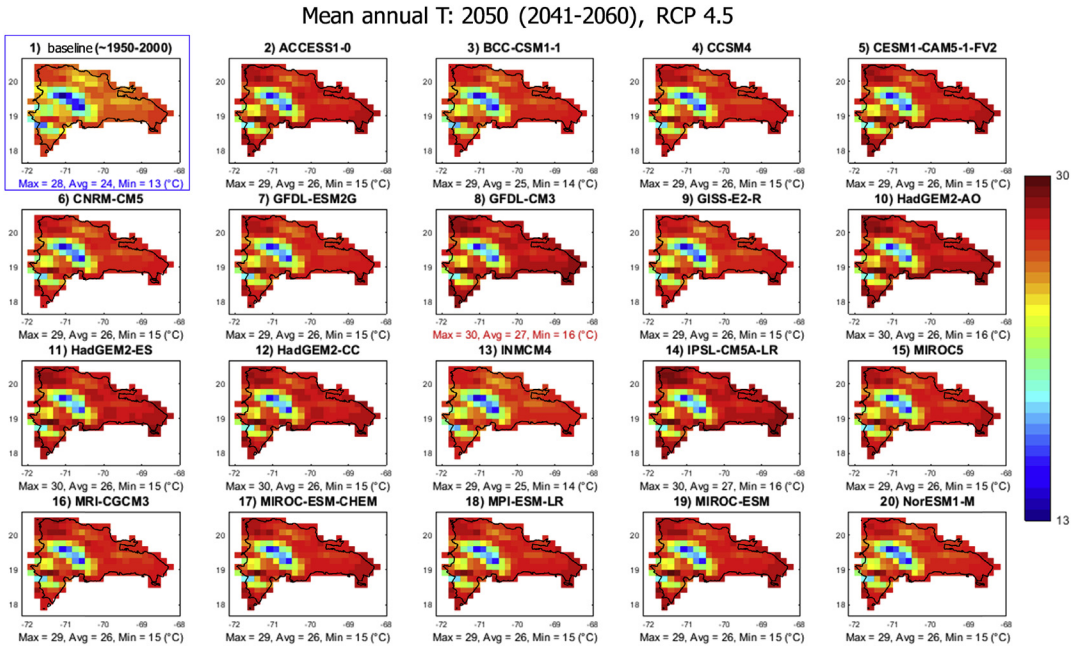

FIGURE 3.6 Spatial distribution of mean annual *T* (°C) over Dominican Republic for the period 2041–60 (2050): baseline and 19 GCMs, and RCP 4.5. *GCM*, General Circulation Model; *RCP*, Representative Concentration Pathway; *T*, temperature.

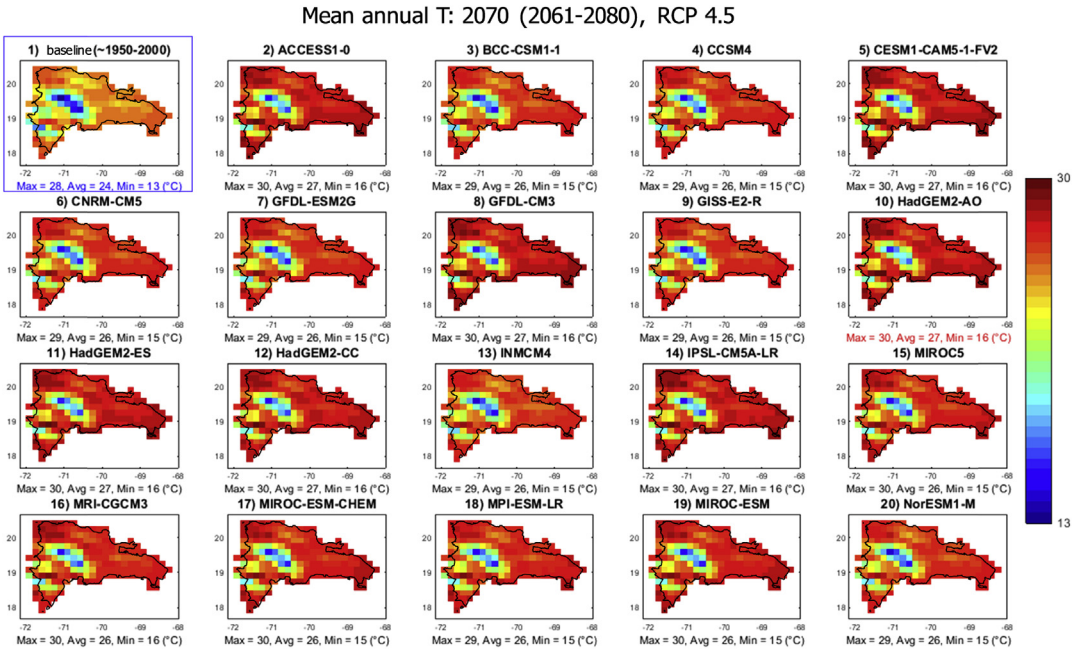

FIGURE 3.7 Spatial distribution of mean annual *T* (°C) over Dominican Republic for the period 2061–80 (2070): baseline and 19 GCMs, and RCP 4.5. *GCM*, General Circulation Model; *RCP*, Representative Concentration Pathway; *T*, temperature.

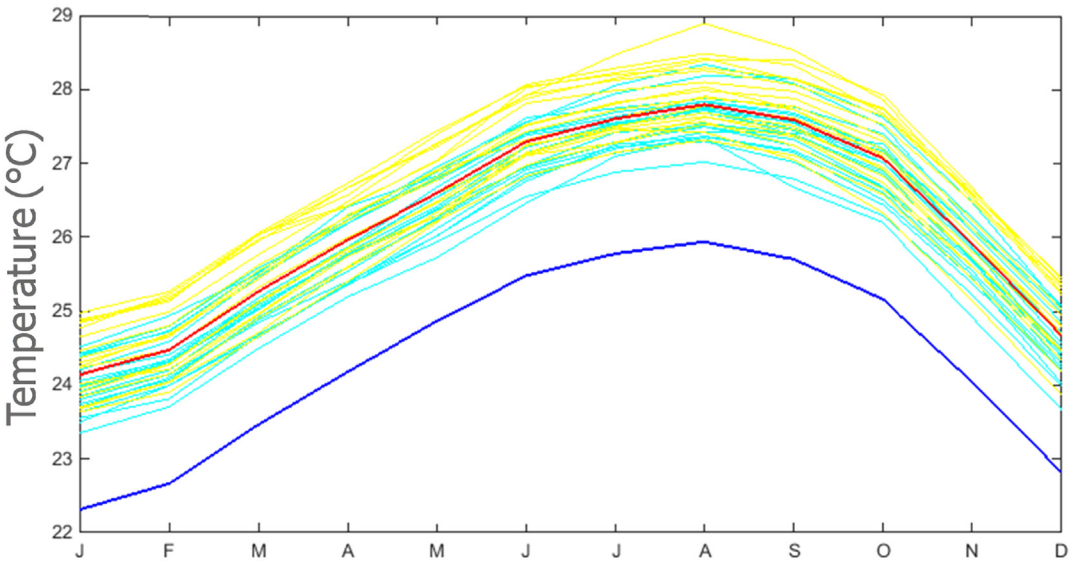

FIGURE 3.8 Dominican Republic: long-term mean *T* of the baseline period (*solid blue line*) and 19 RCP 4.5 projections (*solid red line*). Long-term mean *T* of each projection is also displayed for the period 2041–60 (*solid cyan lines*) and 2061–80 (*solid yellow lines*). *RCP*, Representative Concentration Pathway; *T*, temperature.

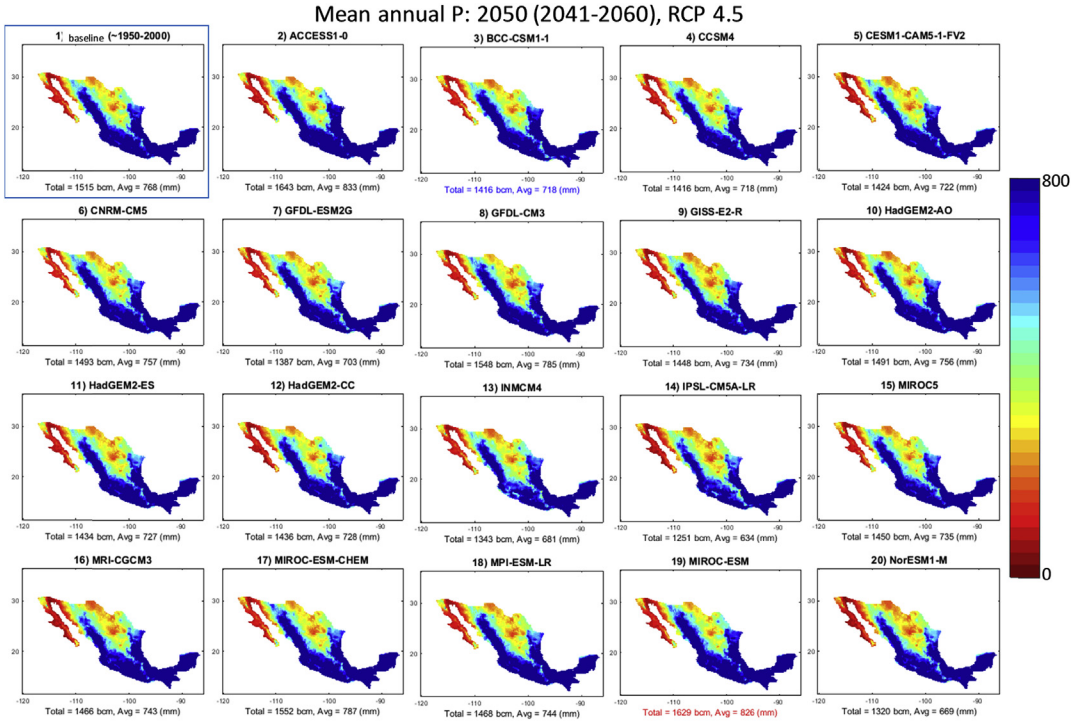

FIGURE 3.9 Spatial distribution of mean annual *P* (mm) over Mexico for the period 2041–60 (2050): baseline and 19 GCMs, and RCP 4.5. *GCM*, General Circulation Model; *P*, precipitation; *RCP*, Representative Concentration Pathway.

8.5. On the other hand, September shows an increase, whose value seems to be lower from route 2.6 to 8.5. July and September are the months with the poorest agreement between GCMs.

Concerning mean annual *T*, Fig. 3.11 shows that most GCMs indicate a rise in the temperatures throughout the country for the period 1941–2060. On the coasts and in the north, the greatest values are observed. Fig. 3.12 also points out an increment in the temporal distribution; values of long-term mean *T* of projections from January to December are larger than those of the baseline period. From June to September, the main increases are observed.

5.3 Amazon Basin

According to the baseline period, the spatial distribution of mean annual *P* shows different values along the basin. The largest appear to be in the northwest and center, followed by the rains in the northwest. The lowest are in the southwest part. According to RCP 4.5, most GCMs indicate a change in the spatial distribution of annual rainfall for

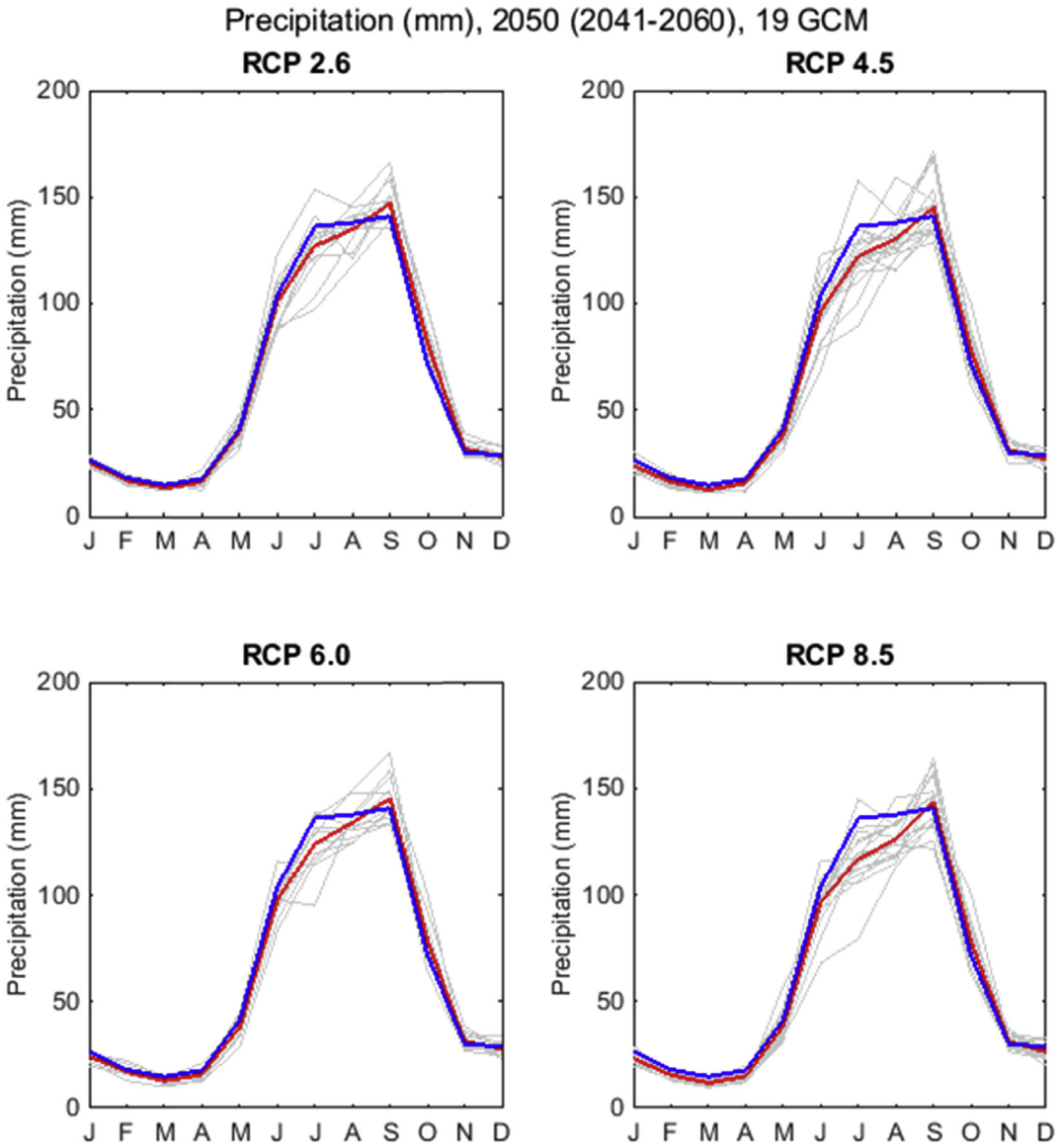

FIGURE 3.10 Mexico: long-term mean *P* of the baseline period (*solid blue line*) and the 19 RCP 2.6, 4.5, 6, and 8.5 projections (*solid red line*). Long-term mean *P* of each projection is also displayed for the period 2041–60 (*solid gray lines*). *P*, Precipitation; *RCP*, Representative Concentration Pathway.

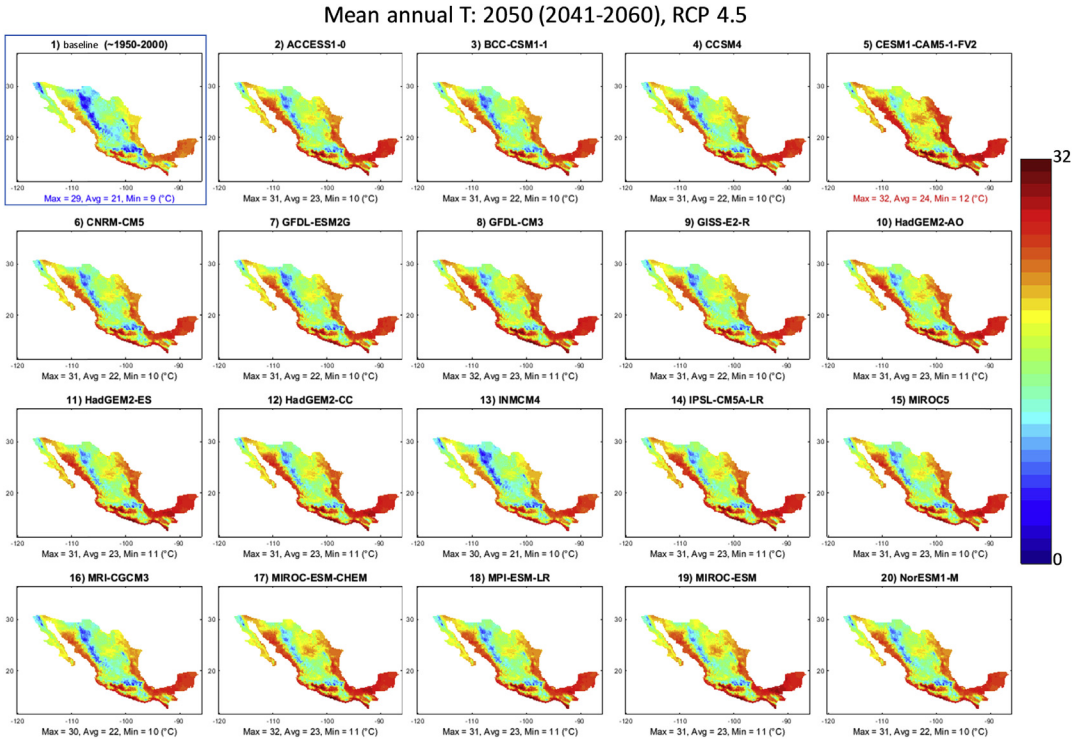

FIGURE 3.11 Spatial distribution of mean annual *T* (°C) over Mexico for the period 2041–60 (2050): baseline and 19 GCMs, and RCP 4.5. *GCM*, General Circulation Model; *RCP*, Representative Concentration Pathway; *T*, temperature.

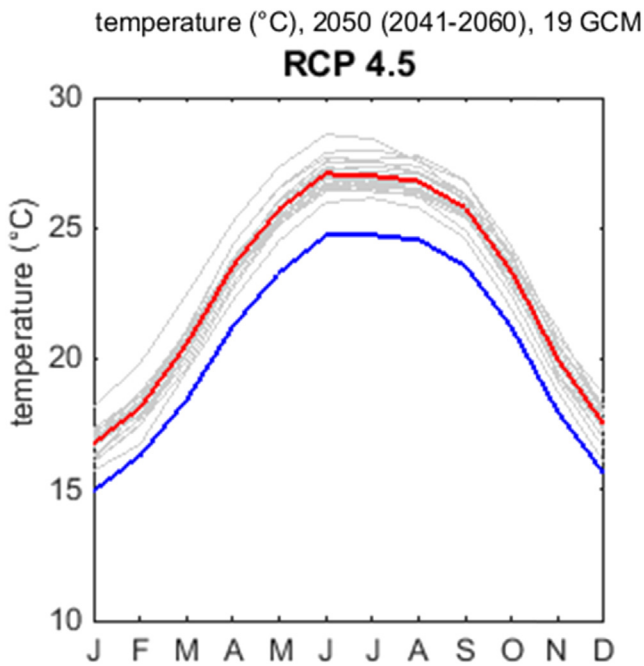

FIGURE 3.12 Mexico: long-term mean *T* of the baseline period (*solid blue line*) and the 19 RCP 4.5 projections (*solid red line*). Long-term mean *P* of each projection is also displayed for the period 2041–60 (*solid gray lines*). *P*, Precipitation; *RCP*, Representative Concentration Pathway; *T*, temperature.

the period 2041–60, mainly in the northwest of the basin, where the values seem to increase (Fig. 3.13).

The long-term mean *P* of projections shows that the values from January to July in general remain, but not the values from August to December, where a drop in the magnitude of rainfall is expected (Fig. 3.15 *left*). The worst agreement between models is observed in October. This is for the period 2041–60.

Most GCMs indicate an increase in temperature throughout the territory of the basin (Fig. 3.14). The northern, eastern, and central parts seem to be the most affected. There is also a rise in the southwest part, where the expected average minimum value is 4 degrees. The long-term mean *T* of projections shows a greater disagreement in every month with respect to rainfall projections. In general, projections indicate an increase in *T* in all months. The poorest agreement is observed in October (Fig. 3.15 *right*).

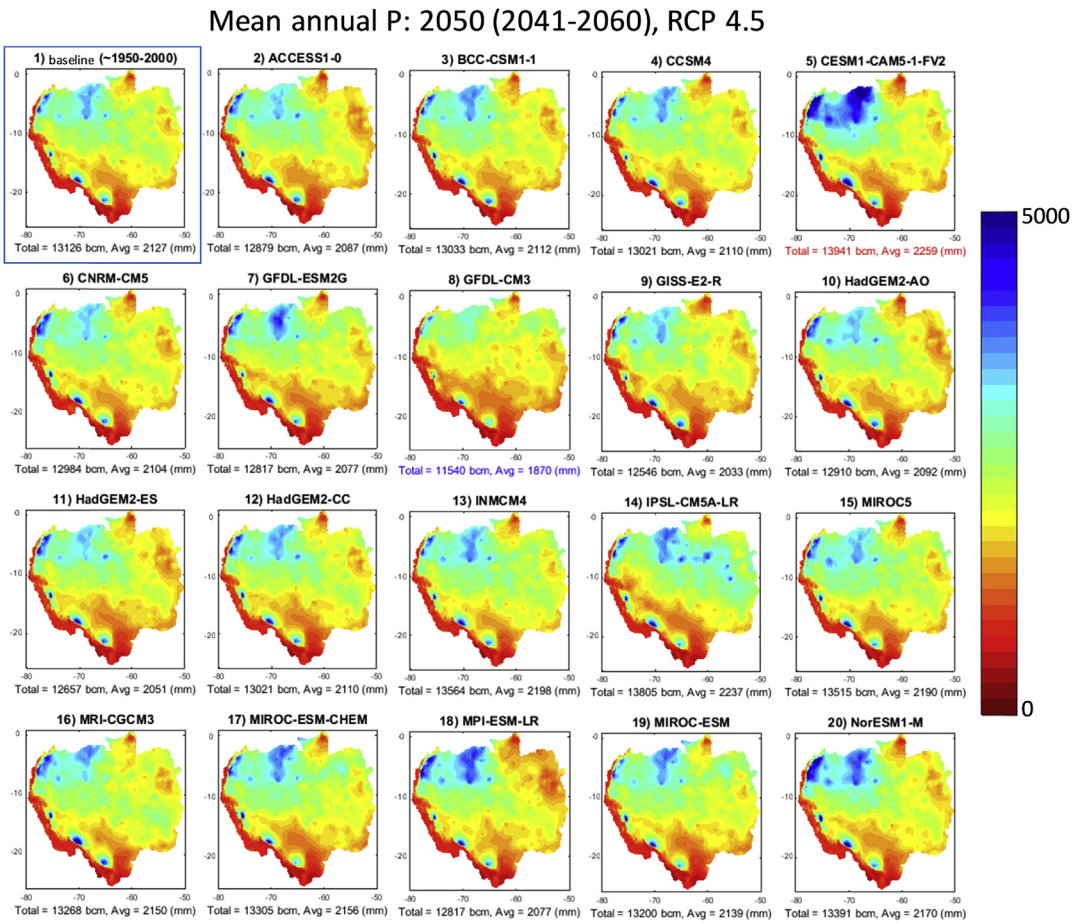

FIGURE 3.13 Spatial distribution of mean annual *P* (mm) over Amazon basin for the period 2041–60 (2050): baseline and 19 GCMs, and RCP 4.5. *GCM*, General Circulation Model; *P*, precipitation; *RCP*, Representative Concentration Pathway.

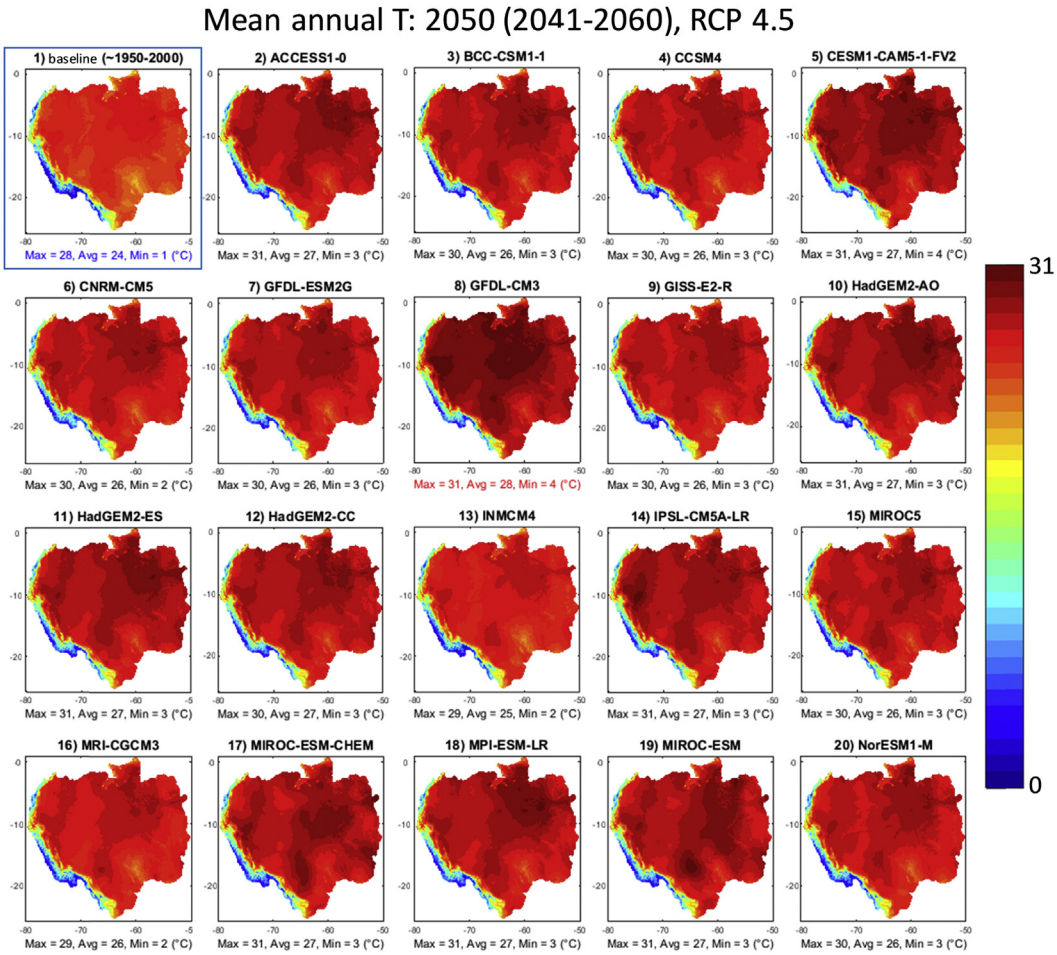

FIGURE 3.14 Spatial distribution of mean annual *T* (°C) over Amazon basin for the period 2041–60 (2050): baseline and 19 GCMs, and RCP 4.5. *GCM*, General Circulation Model; *RCP*, Representative Concentration Pathway; *T*, temperature.

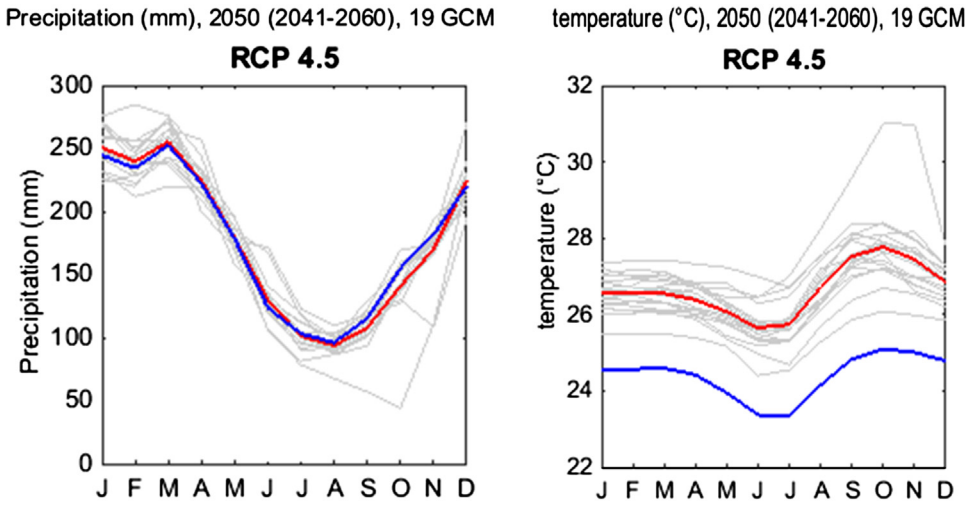

FIGURE 3.15 Amazon basin: long-term mean *P* (*left*) and *T* (*right*) of the baseline period (*solid blue line*) and the 19 RCP 4.5 projections (*solid red line*). Long-term mean *P* of each projection is also displayed for the period 2041–60 (*solid gray lines*). *P*, Precipitation; *RCP*, Representative Concentration Pathway; *T*, temperature.

6. Conclusions

In this chapter the STRIVIng toolbox was introduced. It was shown that STRIVIng is used for the assessment of monthly values in three large-scale applications: Dominican Republic, Mexico, and Amazon basin. STRIVIng was used to:

- Extract and visualize the spatial distribution of annual precipitation and temperature of both baseline and projections.
- Calculate and visualize the long-term mean P and T for months from January to December through line plots.
- Visualize the long-term mean P and T for months from January to December through box-plot charts.

From the application of the toolbox in the case studies, some findings can be drawn.

6.1 Dominican Republic

- For both periods 2050 (2041–60) and 2070 (2061–80), most GCMs agree that the greatest changes in the spatial distribution of P occur on the north coast. While on the border with Haiti, the condition practically remains stable. For the 2050 period, the northern coast will experience an increase in annual rainfall, while a decrease is expected on the southern coast.
- Long-term mean of monthly P will show a decrease in the coming decades, mainly in the months of May to October. June and July are the months that present the greatest fall. The May rainfall projection shows the greatest disagreement among GCMs.
- The country will suffer an increase in the mean annual values of temperature in practically the whole territory for the periods 2041–60 and 2061–80. Only in the central part will the condition remain more stable in both cases.
- An increase of around 2 degrees in the long-term mean of monthly T is observed.

6.2 Mexico

- For the period 2041–60, the spatial distribution of the mean annual P agrees with most of the GCMs. The maximum magnitudes of rainfall are observed on the south coast with the Gulf of Mexico and on the southwest coast with the Pacific Ocean. The lowest values are observed in the north and northwest of the country, on the border with the United States. The area with most disagreement is the southwest coast with the Pacific Ocean.
- According to the four RCPs, the long-term mean of monthly P projections will be of similar magnitude to the baseline period throughout the year, except for the months of June to September, where the models show mainly a drop in values. July is the month that shows the greatest fall; this drop increases from RCP 2.6 to 8.5. On the other hand, September shows an increase, whose value seems to be

lower from route 2.6 to 8.5. July and September are the months with the poorest agreement between GCMs.

- Regarding *T*, results show that most GCMs indicate a rise in temperatures throughout the country for the period 1941–2060. On the coasts and in the north, the greatest values are observed. It is observed that increases in temporal distribution and values of long-term mean *T* projections from January to December are larger than those of the baseline period. The main increases are observed from June to September.

6.3 Amazon Basin

- The spatial distribution of mean annual *P* shows different values along the basin in the baseline period. The largest appear to be in the northwest and center, followed by the rains in the northwest. The lowest are in the southwest part. According to RCP 4.5, most GCMs indicate a change in the spatial distribution of annual rainfall for the period 2041–60, mainly in the northwest of the basin, where the values seem to increase.
- The long-term mean of monthly *P* projections shows that the values from January to July in general remain, but not the values from August to December, where a drop in the magnitude of rainfall is expected. The worst agreement between models is observed in October. This is for the period 2041–60.
- Most GCMs indicate an increase in temperature throughout the territory of the basin. The northern, eastern, and central parts seem to be the most affected. There is also a rise in the southwest part, where the expected average minimum value is 4 degrees. The long-term mean of monthly *T* projections shows a greater disagreement in every month with respect to rainfall projections. In general, projections indicate an increase in *T* in all months. The poorest agreement is observed in October.

The toolbox can be retrieved at https://github.com/hydroinfo4x/STRIVIng.

Acknowledgments

Vitali Díaz thanks the Mexican National Council for Science and Technology (CONACYT) for the study grant 217776/382365. This research was partially financed and supported by the MESCyT and its FONDOCyT program, under the project number 2015-1H1-06 entitled “Impacto del cambio climático en el aprovechamiento sostenible de los recursos hídricos en República Dominicana”. We acknowledge WorldClim data developers for processing the climate projections and for making them freely available.

References

Boer, G.J., 2009. Changes in interannual variability and decadal potential predictability under global warming. Journal of Climate 22 (11), 3098–3109. https://doi.org/10.1175/2008JCLI2835.1.

Coumou, D., Rahmstorf, S., 2012. A decade of weather extremes. Nature Climate Change 2 (7), 491–496. https://doi.org/10.1038/nclimate1452.

Fick, S.E., Hijmans, R.J., 2017. WorldClim 2: new 1-km spatial resolution climate surfaces for global land areas. International Journal of Climatology 37 (12), 4302–4315. https://doi.org/10.1002/joc.5086.

Hawkins, E., Sutton, R., 2009. The potential to narrow uncertainty in regional climate predictions. Bulletin of the American Meteorological Society 90 (8), 1095–1107. https://doi.org/10.1175/2009BAMS2607.1.

IPCC, 2014. In: Core Writing Team, Pachauri, R.K., Meyer, L.A. (Eds.), Climate Change 2014: Synthesis Report. Contribution of Working Groups I, II and III to the Fifth Assessment Report of the Intergovernmental Panel on Climate Change. IPCC, Geneva, Switzerland.

Meehl, G.A., Moss, R., Taylor, K.E., Eyring, V., Stouffer, R.J., Bony, S., Stevens, B., 2014. Climate model intercomparisons: preparing for the next phase. Eos 95 (9), 77–78. https://doi.org/10.1002/2014EO090001.

Meinshausen, M., Smith, S.J., Calvin, K., Daniel, J.S., Kainuma, M.L.T., Lamarque, J., et al., 2011. The RCP greenhouse gas concentrations and their extensions from 1765 to 2300. Climatic Change 109 (1), 213–241. https://doi.org/10.1007/s10584-011-0156-z.

Milly, P.C.D., Dunne, K.A., Vecchia, A.V., 2005. Global pattern of trends in streamflow and water availability in a changing climate. Nature 438 (7066), 347–350. https://doi.org/10.1038/nature04312.

Moss, R.H., Edmonds, J.A., Hibbard, K.A., Manning, M.R., Rose, S.K., Van Vuuren, D.P., et al., 2010. The next generation of scenarios for climate change research and assessment. Nature 463 (7282), 747–756. https://doi.org/10.1038/nature08823.

Najafi, M.R., Moradkhani, H., 2015. Multi-model ensemble analysis of runoff extremes for climate change impact assessments. Journal of Hydrology 525, 352–361. https://doi.org/10.1016/j.jhydrol.2015.03.045.

Taylor, K.E., Stouffer, R.J., Meehl, G.A., 2012. An overview of CMIP5 and the experiment design. Bulletin of the American Meteorological Society 93 (4), 485–498. https://doi.org/10.1175/BAMS-D-11-00094.1.

Trenberth, K.E., 2012. Framing the way to relate climate extremes to climate change. Climatic Change 115 (2), 283–290. https://doi.org/10.1007/s10584-012-0441-5.

Wang, L., Ranasinghe, R., Maskey, S., van Gelder, P.H.A.J.M., Vrijling, J.K., 2016. Comparison of empirical statistical methods for downscaling daily climate projections from CMIP5 GCMs: a case study of the Huai River Basin, China. International Journal of Climatology 36 (1), 145–164. https://doi.org/10.1002/joc.4334.